Automated Micropipette Aspiration of Single Cells

Ehsan Shojaei-Baghini, Yi Zheng & Yu Sun

Annals of Biomedical Engineering
The Journal of the Biomedical Engineering Society

ISSN 0090-6964
Volume 41
Number 6

Ann Biomed Eng (2013) 41:1208-1216
DOI 10.1007/s10439-013-0791-9

Springer

Annals of Biomedical Engineering, Vol. 41, No. 6, June 2013 (© 2013) pp. 1208–1216
DOI: 10.1007/s10439-013-0791-9

Automated Micropipette Aspiration of Single Cells

EHSAN SHOJAEI-BAGHINI,[1] YI ZHENG,[1,2] and YU SUN[1,2,3]

[1]Department of Mechanical and Industrial Engineering, University of Toronto, Toronto, ON, Canada; [2]Institute of Biomaterials and Biomedical Engineering, University of Toronto, Toronto, ON, Canada; and [3]Department of Electrical and Computer Engineering, University of Toronto, Toronto, ON, Canada

(*Received 2 December 2012; accepted 12 March 2013; published online 19 March 2013*)

Associate Editor Scott I Simon oversaw the review of this article.

Abstract—This paper presents a system for mechanically characterizing single cells using automated micropipette aspiration. Using vision-based control and position control, the system controls a micromanipulator, a motorized translation stage, and a custom-built pressure system to position a micropipette (4 μm opening) to approach a cell, form a seal, and aspirate the cell into the micropipette for quantifying the cell's elastic and viscoelastic parameters as well as viscosity. Image processing algorithms were developed to provide controllers with real-time visual feedback and to accurately measure cell deformation behavior on line. Experiments on both solid-like and liquid-like cells demonstrated that the system is capable of efficiently performing single-cell micropipette aspiration and has low operator skill requirements.

Keywords—Robotic cell manipulation, Visual servoing, Biological cell characterization, Micropipette aspiration, Mechanical properties.

INTRODUCTION

The study of living cell mechanics can help gain insights in cell structures and functions.[11] It has been demonstrated that single-cell mechanical characterization can also be useful for investigating disease mechanisms and progression,[3,12,18] since the biomechanical properties of the pathological cells can differ from healthy ones. Mechanical characterization of cells from the pleural fluids of patients revealed that the cancer cells are considerably more deformable than benign cells.[3]

Population-based cell experiments do not permit a thorough examination of the stochastic processes involved in regulating cellular function at the single cell level.[18] The need of investigating biomechanics at cellular level calls for single cell manipulation techniques for studying the complex and dynamic behavior of individual cells. Over the years, many methods have been developed to study mechanical properties of single cells. In atomic force microscopy (AFM), mechanical deformation is induced using the tip of a cantilever. The deflection of the cantilever is used to calculate the applied force. Using this technique, a map of cell stiffness across the cell surface can be generated.[8,11,15,29] In magnetic twisting cytometry (MTC), magnetic beads are attached to the cell surface. Twisting moment induced by the application of a magnetic field causes the cell to deform. Both elastic and viscoelastic properties of cells can be measured using this technique.[1,2,6,15] In optical tweezers (OT), laser beams trap high-refractive-index dielectric beads attached to cells and hence, exert forces to the cells.[11,12,15,21,29] Micropipette aspiration uses a fine hollow needle to aspirate a portion of a cell with vacuum pressure. Geometric changes in cell shape are measured to determine the elastic and viscoelastic properties, and flow resistance of the cell.[5,10,11,22,25,27,29,30] Reported force range of micropipette aspiration is from approximately 10 pN to a few hundreds of nanoNewton. The capability of measuring this large force range is advantageous compared to MTC (0.1–10 pN)[1,2,6] and OT (0.1–1 nN).[15,21] In order for AFM to measure this large force range, AFM cantilevers of different stiffness need to be used. In AFM measurement, the cell is locally deformed by the sharp AFM cantilever tip. In comparison, micropipette aspiration deforms a cell patch in a more global manner, which AFM can achieve only by custom modifying AFM tip geometries (e.g., glue a microsphere onto the cantilever tip).[8,11,15,29] Additionally, micropipette aspiration has low infrastructure requirement.

Conventionally, micropipette aspiration requires well-trained operators to look into the eyepieces of a

Address correspondence to Yu Sun, Department of Mechanical and Industrial Engineering, University of Toronto, Toronto, ON, Canada. Electronic mail: sun@mie.utoronto.ca

microscope, skillfully operate multiple devices to manipulate a cell, control vacuum at proper timings to form a seal between the cell and micropipette opening, and synchronize pressure and video data recording. After manual experiments, the operator determines cell deformations by performing manual measurements on a large amount of recorded images to extract cell deformation parameters.

Micropipette aspiration is a useful technique and has low infrastructure requirement. However, the high skill requirements for operation and the efforts required for tedious, time-consuming post processing of data make the technique difficult and less appealing to use. In contrast, AFM over the past decade has been largely automated. The automated operation of AFM ("point-and-click") is part of the reason why AFM has become a widely adopted tool in cell mechanics. This study aims to prove the feasibility of achieving "point-and-click" operation in micropipette aspiration through the use of automation techniques. In Heinrich and Rawicz[9] and our previous work,[17] image processing algorithms were developed to measure cell deformation. This paper reports an automated system that performs the complete micropipette aspiration procedure *via* computer mouse clicking. The system controls motion control devices based on visual servoing and position control and processes images in real time for tracking features and measuring cell shape changes.

SYSTEM CONTROL

The system (see supplementary Fig. S1) consists of an inverted microscope (Olympus IX81) with a CMOS camera (Basler A601F), a motorized micromanipulator (Siskiyou, 7600 series) with encoder feedback for positioning the micropipette, an XY translation stage (Prior Scientific ProScan II) for positioning cell samples, and a custom-developed pressure system for generating computer-controlled vacuum levels using a differential pressure transducer (Omega PX409-10WDWU5V) to obtain pressure feedback. The host computer runs LabVIEW (National Instruments) programs to control the hardware and to process pressure and image data. Suction pressure ($\Delta P = \rho g \Delta h$) is generated by creating a height difference between the reference and delta tanks (see Fig. 1). Solenoid valves (Fig. 1a) are used to route the fluid for various functions. When pressure is applied to the micropipette tip, all valves are kept open except V2 which connects the high pressure tank to the water circuit (state 2 in Table 1). In the beginning of an experiment when the operator mounts a new micropipette using the back filling method,[9] the trapped air can be forced out by routing the high-pressure pump (Fig. 1b) to the micropipette tip without damaging the transducer (Fig. 1e) or affecting the water levels in reservoirs (state 3 in Table 1). In order to remove the built up bubbles in the water circuit, the high pressure tank is routed to the circuit to push all the gas to open water (state 4 in Table 1).

The positions of the two water tanks were controlled by a standard proportional integral derivative (PID) controller with pressure feedback from the differential pressure transducer (±2 Pa accuracy) as illustrated in Fig. 2a. The measured voltage from the pressure transducer was sampled and converted to pressure units in a PID control loop in LabVIEW. The output of the controller was then converted to steps using a delta–sigma modulator.[26] Figure 3 shows the step responses of the pressure pump. The accuracy the closed-loop controlled pressure system achieves is ±2 Pa, which is limited by the pressure sensor. This pressure inaccuracy can cause errors in the quantification of a cell's mechanical parameters. For instance, according to Eq. (1), assuming an aspiration pressure of −100 Pa, an error of ±2 Pa would result in an error of ±2% in Young's modulus.

The micromanipulator was controlled *via* an image-based look-and-move visual servoing algorithm.[7] The internal closed-loop controller used encoders as input with a sampling rate of 1 kHz, whereas the visual servoing controller had a low sampling rate of 30 Hz

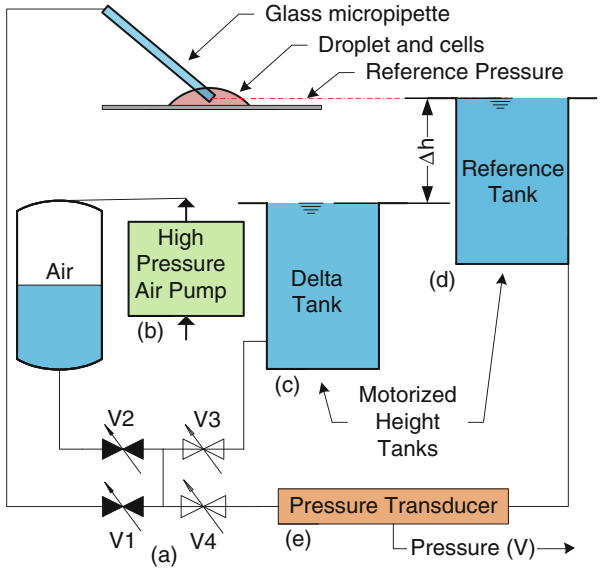

FIGURE 1. Digital pressure pump. (a) Solenoid valves are used in routing fluid. (b) High pressure air pump is used to remove trapped air from a newly mounted micropipette. (c) Delta tank moves vertically to generate pressure. (d) Reference tank moves vertically to balance the pressure in delta tank. (e) Differential pressure transducer outputs the pressure difference between delta and reference tanks in volts.

TABLE 1. Valve states in the digital pressure system.

State	Description	V1	V2	V3	V4
1	Sense pressure	C	O	O	O
2	Sense and apply pressure	O	C	O	O
3	Route high pressure to micropipette only	O	O	C	C
4	Route high pressure to delta tank only	C	O	O	C

O and C represent open and close, respectively.

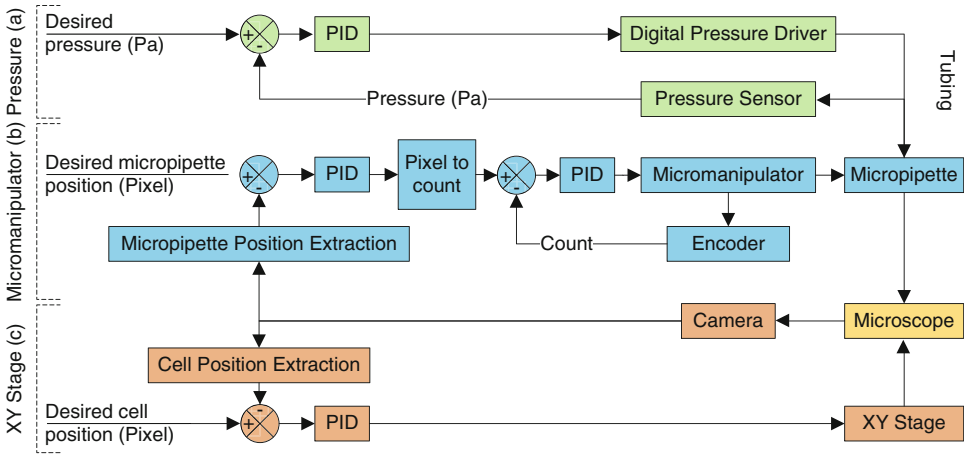

FIGURE 2. System control architecture. (a) PID position controller for controlling the pressure system. (b) Image-based look-and-move visual servoing controller for controlling the micromanipulator. (c) PID position controller for controlling the motorized XY translation stage.

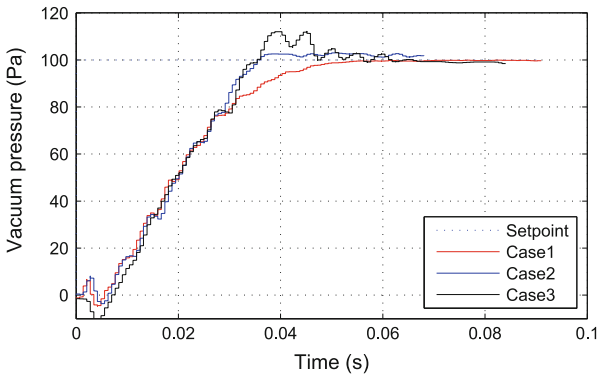

FIGURE 3. Pressure pump response to a step input of 100 Pa (vacuum pressure). Case 1: over-damped; Case 2: critically damped; Case 3: under-damped.

(Fig. 2b). Gain scheduling is a popular nonlinear controller design approach for improving the performance of a PID controller by adjusting PID gain parameters.[13,24] In the implemented controller, the gain scheduler switches between two sets of gain parameters based on the magnitude of the error. In large errors (>3 μm), the algorithm uses a fast P controller (Fig. 4a); However, in small errors (≤ 3 μm) the algorithm uses a relaxed and slower PI controller. The threshold of 3 μm was experimentally chosen in order to obtain satisfactory positioning response and visual tracking results. Using two sets of PID gain parameters, allows fast paced motions for large distances as well as slow motion near the target where tracking the micropipette tip is performed more accurately due to absence of motion blur. This ensures a smooth motion and minimizes micropipette vibrations (Fig. 4b). Cells in a standard Petri dish are placed on the motorized XY translation stage that is also controlled *via* image-based look-and-move visual servoing, as shown in Fig. 2c. The PID controller sends velocity commands to the stage amplifier.

VISUAL TRACKING

Micropipette Tracking

The micropipette tip is visually tracked using an optimized rotation-invariant normalized cross-correlation (NCC) method. The basic NCC algorithm was described in Lewis.[14] A template of the micropipette tip (Fig. 5a) is cross-correlated with the current frame of image to locate the best match within a search area. The selection of a template is required only when a new

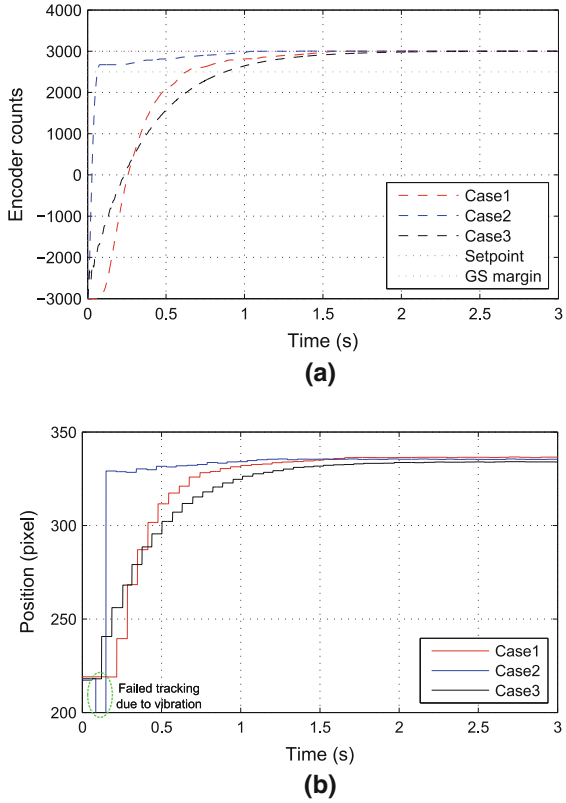

FIGURE 4. Micropipette controller. (a) Three cases of PID gains and implemented gain scheduling. Micromanipulator response to a step input of 3000 counts. The gain scheduling margin (GS) is 500 counts. Case 1 is critically damped. Case 2 is critically damped with a relaxed PI controller for small error magnitudes. Case 3 is over-damped. (b) The visual tracking results of the cases. Despite the fast response in Case 2, the induced vibration compromises the visual tracking performance. Thus, a slower set of gains (Case 1) is chosen to provide a smooth, vibration-free motion at the micropipette tip. Micropipette visual tracking results. Due to the induced mechanical vibration in Case 2, the tracking algorithm fails to locate the micropipette.

micropipette is mounted on the micromanipulator in the beginning of an experiment. The opening of the template is also manually selected for later elongation measurement at this stage (Fig. 5b). Once the template is selected, the search area is limited to the proximity of the last known location of the micropipette from the previous frame. This method reduces the search time. The normalized cross-correlation algorithm determines the location and the angle of the matched template (x, y, α), as shown in Fig. 5c.

Cell Tracking

There are typically several cells present within a field of view. Thus, the cell tracking algorithm requires the user to indicate which cell is the target for characterization *via* one computer mouse click anywhere on top of the target cell (see green cross in Fig. 6a).

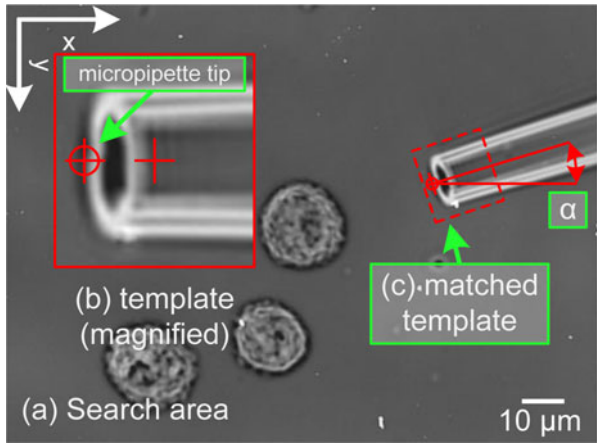

FIGURE 5. Micropipette tracking. (a) Search with the normalized cross-correlation algorithm within the search area. (b) User selects a template containing the micropipette tip and defines the micropipette tip. (c) Matched template location and angle (x, y, α).

The cell tracking algorithm uses binary morphology techniques[4] to determine the position of the cell. The system then forms a region of interest (ROI) that is binarized with the Otsu adaptive thresholding method (Fig. 6b). ROI is defined by centering the inside area of the micropipette after the template matching algorithm locates the micropipette. Close binary operation is used to create a smooth object on the outside (Fig. 6c). Convex hull is used to obtain the cell's envelope (Fig. 6d), and objects with small areas are removed (Fig. 6e). The system determines the position and radius of the cell (x, y, R_c) (Fig. 6f) using least squares fitting.

Aspiration Length Tracking

When a cell is aspirated into the micropipette, an ROI is formed to include the inside of the micropipette, as shown in Fig. 7a. The extracted ROI is then convolved with a standard 5×5 West Sobel kernel to eliminate the vertical edges and enhance the horizontal contours (Fig. 7b). The result of the gradient filter is binarized using the Otsu method, as shown in Fig. 7c. At this stage the image consists of many binary blubs from which the cell contour is extracted. Area, center of mass, and bounding rectangle for each blub are calculated. After binary morphology close operation, the objects found in the image are filtered according to two criteria: (1) an object is removed if its area is smaller than a threshold value; and (2) an object is removed if the center of mass (center of area of each blub on the binary image) is not in the "safe zone" (i.e., inside the micropipette), as shown in Fig. 7c. The first criterion filters out noises and small moving background debris. In this criterion, the threshold value of 8 μm was experimentally selected based on

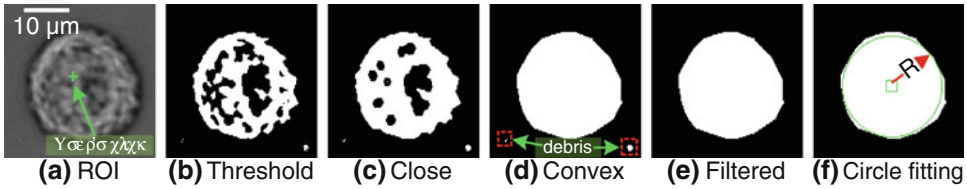

FIGURE 6. Cell tracking. (a) ROI formed around user's click (green cross). (b) Binarized image with the Otsu adaptive thresholding method. (c) Morphological close operation creates a smooth object. (d) Morphological convex operation fills the holes and creates an envelope of the cell. (e) Noise removal based on object area. (f) Least square fitting to obtain a circle (x, y, R_c).

FIGURE 7. Cell aspiration length tracking. (a) ROI containing the inside of the micropipette. (b) Sobel filter is used to enhance the edges and remove vertical edges. (c) The tracked aspiration length is labeled in between the two green lines. The green line on the right is the position of the micropipette opening, and the green line on the left is the leading edge of the cell aspirated into the micropipette. The area between the dashed red lines is termed "safe zone".

the diameter of cells for aspiration. The second criterion ensures that the attached debris to the pipette walls are not recognized as cell contour, and the "safe zone" is defined in the center line of the micropipette where the cell contour location is expected. The beginning of the left most edge is recognized as the protruded cell contour (see green line in Fig. 7c). The aspiration length is defined as the distance between the tracked protrusion and the micropipette opening (see red arrow in Fig. 7c). Details on experimental protocol are presented in the supplementary materials (Fig. S3).

RESULTS AND DISCUSSION

For validation, the automated system was used to measure the elastic and viscoelastic properties of solid-like cells (porcine aortic valve interstitial cells, PAVICs) and measure the viscosity of liquid-like cells (human promyelocytic leukemia cells, HL-60). It has been shown that PAVICs determine the regulatory heart valve function.[20,28] Leukocytes are known to play a significant role in the immune system defending human body against many diseases. Less deformable cells induce impairment to the circulation to the eye and the central nervous system causing damage to such organs.[32] The PAVIC and HL-60 cells were chosen because the characterization results of these cells using manual micropipette aspiration are available in the literature,[17,20,25,31] which permitted the comparison of the results from our automated system and those previously published results.

The PAVICs used in the experiments were harvested from aortic valve leaflets from porcine. The PAVICs were re-suspended in standard tissue culture medium (DMEM supplemented with 10% FBS and 1% antibiotics). When the cultured cells were confluent, the cells were re-suspended in standard DMEM using trypsinization method. The human promyelocytic leukemia cells (HL-60) used in the experiments were purchased from ATCC (CCL-240), which were obtained by leukopheresis from a 36-year-old female with acute promyelocytic leukemia. The cells were subcultured by replacement of medium (as recommended by ATCC) every 2 days.

Prior to automated cell testing, micropipette were made from borosilicate glass tubes with OD of 1.0 mm and ID of 0.75 mm (Sutter Instrument). Each glass pipette was first pulled using a micropipette puller (Sutter Instrument). Following that, the tips were fractured to create an inner diameter of 2–5 μm using a micro-forge (Technical Products International, Inc.). The tips of the micropipettes were bent 45° using the micro-forge.

The system performed cell aspiration according to the following protocol consisting of five steps (Fig. S2): (1) find and home (move the pipette opening to the top-right corner of the field of view (original point)) micropipette based on a pre-defined micropipette template; (2) center a user-selected cell in the field of view; (3) create a seal between cell and micropipette tip based on a pre-defined pressure, P_{seal}; (4) perform aspiration; and (5) process data. There are three types of experiments that a user can choose to conduct: (a) characterization of elastic properties of solid-like cells; (b) characterization of viscoelastic properties for solid-like cells; (c) viscous properties of liquid-like cells. When homing the micropipette, the pipette tip is only moved in-plane. Since system drift caused by environmental noise (e.g., temperature and vibration) was small (~2 μm in 10 min), the pipette tip remained in the focal plane. The concentration of the cell suspension in the experiments was kept relatively low; therefore, the chance of encountering other cells en route was low.

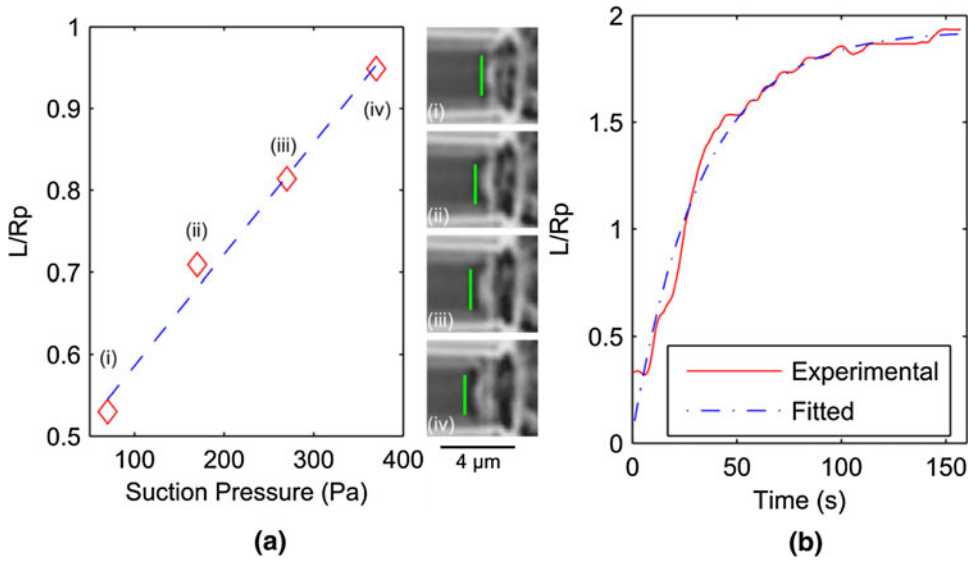

FIGURE 8. Elastic and viscoelastic responses of PAVICs. L is the aspiration length and R_p is the radius of the micropipette. (a) Elastic response of a PAVIC, where (i)–(iv) are equilibrium points at the end of 100 s intervals. (b) Viscoelastic response of a PAVIC. A step pressure of −400 Pa was applied for 150 s.

When the pipette tip occasionally encountered other cells en route, the cells were simply pushed away.

Elastic Characterization

In order to measure a cell's Young's modulus, the system applied a series of small pressure steps (four steps of −100 Pa) to the cell with an interval of 100 s *via* the digital pressure system with an initial seal pressure of −70 Pa. The aspiration length (L) and step pressure (ΔP) are related by the half space model[25]

$$\frac{L}{R_p} = \frac{3\Delta P}{2\pi E}\Phi_{p(\eta)} \tag{1}$$

where E is the Young's modulus, Φ_p for our used micropipette is approximately 2.1, and η is the wall parameter. The aspiration length, L and suction pressure, ΔP (Fig. 8a) at the end of each 100-s interval were used for linear regression to obtain the Young's modulus from the slope of the fitted line. A robust linear regression was used to eliminate the effect of outliers. The determined Young's modulus value for the tested PAVICs is 358.7 ± 192 Pa ($n = 30$). This result is in agreement with our previous results (345.8 ± 142.5 Pa) from manual testing[17] and agrees well with the results reported in Merryman *et al.*[20]

Viscoelastic Characterization

We also used the system for quantifying viscoelastic properties of the PAVIC cells. In viscoelastic characterization, the system applied to the cell a large step pressure (−400 Pa) for 150 s. In this period, the system on-line measured the cell aspiration length, $L(t)$, which is related to step pressure input (h) by the Kelvin model.[17]

$$L(t) = L_s\left[1 - \frac{k_2}{k_1 - k_2}\exp\left(\frac{-t}{\tau}\right)\right]h(t) \tag{2}$$

where L_s is the aspiration length at the end of the interval. Using least-squares nonlinear fitting, $L(t)$ was fitted to the recorded data to determine k_1, k_2, and τ (Fig. 8b), where k_1 and k_2 are the elastic constants of a standard linear body, and τ is the time constant. The results are summarized in Table 2 together with the previously reported values from manual testing.[25] A two group T test was performed on the elastic and viscoelastic parameters of PAVICs determined from automated measurement and manual measurements.[17] The p-values are consistently higher than 0.05 (p-values of Young's modulus, k_1, k_2, and τ are: 0.86, 0.27, 0.29, and 0.52), indicating that no significant difference exists between automated and manual measurements. It is worth noting that Eqs. (1) and (2) used for extracting Young's modulus and viscoelastic properties is based on the assumption that the cells are isotropic homogeneous incompressible elastic solid or viscoelastic solid bodies.[16] There also exist other models, for instance, the Boltzmann Standard Linear Solid model for accounting for a finite rate at which pressure is applied.[19,23] The primary purpose of this work is to verify the validity of the automated micropipette aspiration system; hence, it was necessary to compare the results from the automated system with those from

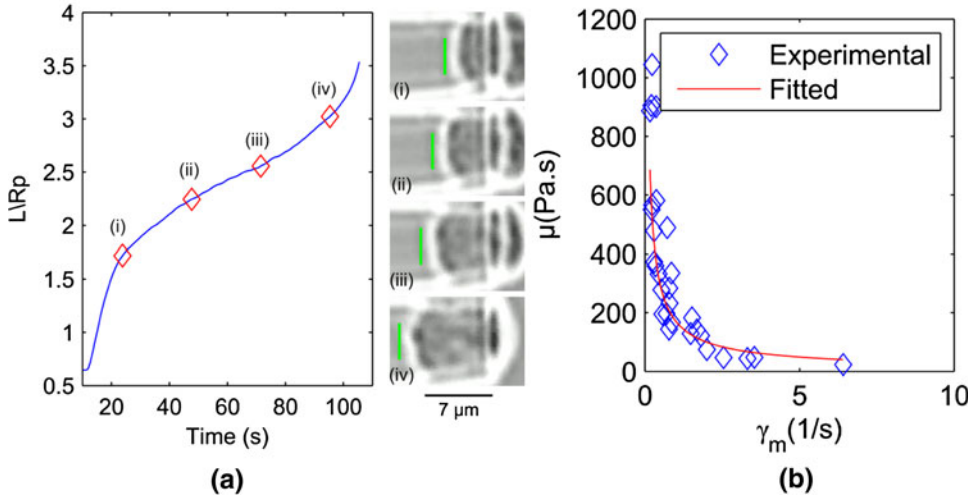

FIGURE 9. Viscous properties of HL-60 cells. (a) Viscous response of an HL-60 cell to a step pressure of −270 Pa. (i)–(iv) show the cell at various time instances. *L* is the aspiration length and R_p is the radius of the micropipette. (b) Cytoplasmic viscosity as a function of mean shear rate γ_m. Step pressure varied from −700 to −220 Pa (n = 30).

TABLE 2. Determined viscoelastic parameters of PAVICs.

Viscoelastic parameters	k_1 (Pa)	k_2 (Pa)	τ (Pa s)
Automated MA results ($n = 25$)	189.6 ± 71.3	270.4 ± 68.6	40.0 ± 34.2
Literature reported values[17]	153.8 ± 59.9	310.1 ± 70.4	45.3 ± 11.6

previously reported studies on the same types of cells. Since raw data are not directly comparable, and the majority of previously published work used the model shown in Eqs. (1) and (2), we used the same model, despite its limitations, to process our experimental data in order to verify our automated technique.

Viscosity Characterization

To quantify viscosity of liquid-like cells, the automated micropipette aspiration system applied step pressures ranging from −700 to −220 Pa for 150 s to HL-60 cells. In this period, the system automatically measured aspiration lengths, $L(t)$, as shown in Fig. 9. The characteristic viscosity of HL-60 cells was calculated based on the methodology used in Tsai *et al.*[31,32]

$$\mu = \mu_c \left(\frac{\gamma_m}{\gamma_c}\right)^{-b} \tag{3}$$

where μ is the cytoplasmic viscosity, γ_m is the mean shear rate during cell entry into the micropipette, μ_c is the characteristic viscosity at the characteristic shear rate γ_c, and b is a material coefficient. In this study, γ_c was set to $1\ s^{-1}$. Characterization results are $\mu_c = 171.35 \pm 13.04$ Pa s, and $b = 0.78 \pm 0.08$ for HL-60 cells ($n = 30$). These values are in agreement with the previously reported values[32] ($\mu_c = 197 \pm 25$ Pa s, and $b = 0.53 \pm 0.02$).

DISCUSSION

For performance comparison, manual micropipette aspiration was also performed by a proficient operator. In manual operation, the user looked into the eyepieces of the microscope and controlled the micropipette positions using a joystick. Comparing the speed of locating and homing the micropipette, the system was at least two times faster than the proficient operator (19 vs. ~60 s). The system was also at least twice as fast in forming a seal between a cell and the micropipette (23 vs. ~52 s). The time taken in the cell aspiration step was comparable since sufficient waiting time was required for cells to respond; however, pressure profiles were generated more accurately by the closed-loop controlled pressure pump in the automated system. The accurately generated pressure profiles significantly facilitated seal formation and reduced the inconsistency in human operation. It would take much longer for less trained users in these steps in manual operation, while the automated system's performance and operation speed are user independent. In image processing, the system determined cell deformation

parameters during cell aspiration in real time without the need for tedious, lengthy post processing. In comparison, it took the proficient user averagely 2 min per cell to manually make measurements in recorded images for elastic measurements and approximately 2 h for viscoelastic characterization due to the high number of images captured.

Future improvement of the system necessitates a higher degree of automation to further lower operator skill requirements. For example, locating the micropipette tip is a prerequisite step in micropipette aspiration. The tiny tip is difficult to locate, particularly under high magnifications in microscopy imaging. When the tip collides into other objects (e.g., substrate) during the process of locating the tip, the tip can be easily damaged. A higher degree of automation would increase the practical value of the micropipette aspiration system.

CONCLUSION

This paper presented an automated micropipette aspiration system. The system performance was evaluated by characterizing elastic and viscoelastic properties of PAVICs and HL-60 cells representing solid and liquid-like cell models. Cell characterization results are in agreement with those reported in the literature. Experiments demonstrate that the system enables single-cell micropipette aspiration with a higher efficiency and higher accuracy. System performance is operator skill independent and is achieved by "point-and-click."

ELECTRONIC SUPPLEMENTARY MATERIAL

The online version of this article (doi:10.1007/s10439-013-0791-9) contains supplementary material, which is available to authorized users.

ACKNOWLEDGMENTS

The authors thank John Nguyen for helpful discussions and thank Haijiao Liu and Prof. Craig Simmons for PAVIC cell preparation. The authors acknowledge financial support from the Natural Sciences and Engineering Research Council of Canada and the Canada Research Chairs Program.

CONFLICT OF INTEREST

The authors confirm that there are no known conflicts of interest associated with this publication and there has been no significant financial support for this work that could have influenced its outcome.

REFERENCES

[1]An, S. S., B. Fabry, X. Trepat, N. Wang, and J. J. Fredberg. Do biophysical properties of the airway smooth muscle in culture predict airway hyperresponsiveness? *Am. J. Respir. Cell Mol. Biol.* 35(1):55–64, 2006.
[2]Bao, G., and S. Suresh. Cell and molecular mechanics of biological materials. *Nat. Mater.* 2(11):715–725, 2003.
[3]Cross, S. E., Y.-S. Jin, J. Rao, and J. K. Gimzewski. Nanomechanical analysis of cells from cancer patients. *Nat. Nanotechnol.* 2(12):780–783, 2007.
[4]Dougherty, E. R., and R. A. Lotufo. Hands-on Morphological Image Processing. Bellingham, WA: SPIE, 2003.
[5]Evans, E., and A. Yeung. Apparent viscosity and cortical tension of blood granulocytes determined by micropipet aspiration. *Biophys. J.* 56(1):151–160, 1989.
[6]Fabry, B., G. Maksym, J. Butler, M. Glogauer, D. Navajas, and J. Fredberg. Scaling the microrheology of living cells. *Phys. Rev. Lett.* 87(14):1–4, 2001.
[7]Hashimoto, K. A review on vision-based control of robot manipulators. *Adv. Robotics* 17(10):969–991, 2003.
[8]Haupt, B. J., A. E. Pelling, and M. A. Horton. Integrated confocal and scanning probe microscopy for biomedical research. *Sci. World J.* 6:1609–1618, 2006.
[9]Heinrich, V., and W. Rawicz. Automated, high-resolution micropipet aspiration reveals new insight into the physical properties of fluid membranes. *Langmuir* 21(5):1962–1971, 2005.
[10]Hochmuth, R. M. Micropipette aspiration of living cells. *J. Biomech.* 33(1):15–22, 2000.
[11]Kim, D.-H., P. K. Wong, J. Park, A. Levchenko, and Y. Sun. Microengineered platforms for cell mechanobiology. *Annu. Rev. Biomed. Eng.* 11:203–233, 2009.
[12]Lee, G. Y. H., and C. T. Lim. Biomechanics approaches to studying human diseases. *Trends Biotechnol.* 25(3):111–118, 2007.
[13]Leith, D. J., and W. E. Leithead. Survey of gain-scheduling analysis and design. *Int. J. Control* 73(11):1001–1025, 2000.
[14]Lewis, J. P. Fast normalized cross-correlation. *Vis. Interface* 10(1):120–123, 1995.
[15]Lim, C. T., E. H. Zhou, A. Li, S. R. K. Vedula, and H. X. Fu. Experimental techniques for single cell and single molecule biomechanics. *Mater. Sci. Eng. C* 26(8):1278–1288, 2006.
[16]Lim, C. T., E. H. Zhou, and S. T. Quek. Mechanical models for living cells—a review. *J. Biomech.* 39:195–216, 2006.
[17]Liu, X., Y. Wang, and Y. Sun. Cell contour tracking and data synchronization for real-time, high-accuracy micropipette aspiration. *IEEE Trans. Autom. Sci. Eng.* 6(3):536–543, 2009.
[18]Lu, Z., C. Moraes, G. Ye, C. A. Simmons, and Y. Sun. Single cell deposition and patterning with a robotic system. *PLoS ONE* 5(10):e13542, 2010.
[19]Merryman, W. D., P. D. Bieniek, F. Guilak, and M. S. Sacks. Viscoelastic properties of the aortic valve interstitial cell. *J. Biomech. Eng.* 131:041005, 2009.
[20]Merryman, W. D., I. Youn, H. D. Lukoff, P. M. Krueger, F. Guilak, R. A. Hopkins, and M. S. Sacks. Correlation between heart valve interstitial cell stiffness and transval-

vular pressure: implications for collagen biosynthesis. *Am. J. Physiol. Heart Circ. Physiol.* 290(1):H224–H231, 2006.
[21]Mills, J. P., L. Qie, M. Dao, C. T. Lim, and S. Suresh. Nonlinear elastic and viscoelastic deformation of the human red blood cell with optical tweezers. *Mech. Chem. Biosyst.* 1(3):169–180, 2004.
[22]Needham, D., and R. M. Hochmuth. Rapid flow of passive neutrophils into a 4 microns pipet and measurement of cytoplasmic viscosity. *J. Biomech. Eng.* 112(3):269–276, 1990.
[23]Pravincumar, P., D. L. Bader, and M. M. Knight. Viscoelastic cell mechanics and actin remodelling are dependent on the rate of applied pressure. *PLoS ONE* 7:e43938, 2012.
[24]Rugh, W. J., and J. S. Shamma. Research on gain scheduling. *Automatica* 36(10):1401–1425, 2000.
[25]Sato, M., D. P. Theret, L. T. Wheeler, N. Ohshima, and R. M. Nerem. Application of the micropipette technique to the measurement of cultured porcine aortic endothelial cell viscoelastic properties. *J. Biomech. Eng.* 112(3):263, 1990.
[26]Schreier, R., and G. C. Temes. Understanding Delta–Sigma Data Converters, Vol. 22. Piscataway, NJ: Wiley-IEEE Press, p. 464, 2005.
[27]Shao, J. Y., and R. M. Hochmuth. The resistance to flow of individual human neutrophils in glass capillary tubes with diameters between 4.65 and 7.75 microns. *Microcirculation* 4(1):61–74, 1997.
[28]Simmons, C. A. Aortic valve mechanics: an emerging role for the endothelium. *J. Am. Coll. Cardiol.* 53(16):1456–1458, 2009.
[29]Suresh, S. Biomechanics and biophysics of cancer cells. *Acta Biomater.* 3(4):413–438, 2007.
[30]Theret, D. P., M. J. Levesque, M. Sato, R. M. Nerem, and L. T. Wheeler. The application of a homogeneous half-space model in the analysis of endothelial cell micropipette measurements. *J. Biomech. Eng.* 110(3):190–199, 1988.
[31]Tsai, M. A., R. S. Frank, and R. E. Waugh. Passive mechanical behavior of human neutrophils: power-law fluid. *Biophys. J.* 65(5):2078–2088, 1993.
[32]Tsai, M. A., R. E. Waugh, and P. C. Keng. Cell cycle-dependence of HL-60 cell deformability. *Biophys. J.* 70(4): 2023–2029, 1996.